Loss mechanisms in TiN high impedance superconducting microwave circuits

Kazi Rafsanjani Amin, Carine Ladner, Guillaume Jourdan, Sébastien Hentz, Nicolas Roch, Julien Renard

Loss mechanisms in TiN high impedance superconducting microwave circuits

Kazi Rafsanjani Amin,[1,2] Carine Ladner,[2] Guillaume Jourdan,[2] Sebastien Hentz,[2] Nicolas Roch,[1] and Julien Renard[1]

[1] *Univ. Grenoble Alpes, CNRS, Grenoble INP, Institut Neél, 38000 Grenoble, France*
[2] *Univ. Grenoble Alpes, CEA, LETI, 38000 Grenoble, France*

Aluminium based platforms have allowed to reach major milestones for superconducting quantum circuits. For the next generation of devices, materials that are able to maintain low microwave losses while providing new functionalities, such as large kinetic inductance or compatibility with CMOS platform are sought for. Here we report on a combined direct current (DC) and microwave investigation of titanium nitride films of different thicknesses grown using CMOS compatible methods. For microwave resonators made of 3 nm thick TiN, we measured large kinetic inductance $L_K \sim 240$ pH/sq, high mode impedance of ~ 4.2 kΩ while maintaining microwave quality factor $\sim 10^5$ in the single photon limit. We present an in-depth study of the microwave loss mechanisms in these devices that indicates the importance of quasiparticles and provide insights for further improvement.

After several decades of intense research, major developments happened in quantum technologies. Superconducting circuits, developped primarily using aluminium based technology, are one of the leading platforms for quantum computing to date, with the major milestone of computational advantage being reported recently[1, 2]. Beyond quantum computing, superconducting microwave devices comprising qubits and microwave resonators are also used to study a wide variety of fundamental problems such as ultra-strong light-matter coupling [3, 4], many-body quantum physics [5, 6], quantum simulation of interactions in a lattice [7–9], or topological protection [10, 11].

With the large complexity of addressing a real-life problem, integration of a large number of qubits and resonators while keeping very long coherence in a quantum processor becomes inevitable. In this context, a lossless, high inductance element, called superinductance [12], whose impedance is comparable to, or larger than, the resistance quantum $R_Q = h/4e^2 \approx 6.5$ kΩ at microwave frequencies, is a promising building block. It naturally provides large integration by drastically reducing device footprint, and is also a key feature to realize protection from decoherence [13–15] or to achieve strong light-matter coupling [16, 17]. However, while the conventional approach of building a superinductance using large arrays of Al-AlO_X based Josephson junctions (JJ)s [18–20] have already enabled exploring rich physics, the fabrication technology is incompatible with scalable platforms, and becomes increasingly challenging upon increasing the number of JJs in the array. This has recently motivated the study of alternative new materials for fabrication of scalable and high-coherence superconducting quantum devices [21–23]. Fabrication of superinductances using kinetic inductance of disordered superconductor thin films became a promising alternative to Al, and different materials such as TiN [24–27], NbTiN [28], NbN [29, 30], AlO_x [21, 31, 32], InO_x [33, 34], doped Si [35], W [36] have been investigated.

In this letter we demonstrate TiN superconducting circuits fabricated with a VLSI, CMOS-compatible process featuring, at the same time high film quality, ultra-low microwave losses down to the quantum regime and high kinetic inductance. Microwave electrodynamics of disordered TiN [37, 38], as well as study of low-frequency resistivity investigating different aspects, such as effect of magnetic disorders on the superconducting behavior [39], have been already reported in TiN and NbTiN. Very high quality resonators, with internal quality factor at high electric field as large as 10^7 [25, 26] have been realized using thick films of TiN and various fabrication techniques [27, 39–41]. NbTiN-based nanowire superinductances have been used to demonstrate a fluxonium qubit [42]. However, with reducing thickness, which is needed to reach large kinetic inductances, and increasing amount of disorder, the microwave losses and sample variability increase, compromising future integration in large scale devices. Hence, a detailed understanding of microwave loss mechanisms in these emerging materials is highly needed [43]. We investigate microwave properties of disordered TiN thin films down to very low thickness, and we identify the dominating microwave loss mechanisms.

TiN films of different thicknesses t were deposited, using VLSI CMOS-compatible physical vapour deposition (PVD) method on high-resistivity, 725 μm thick silicon (100) wafer of 200 mm diameters. Excellent homogeniety and uniformity of film characteristics were achieved as a result of VLSI process [Supplementary section-I]. We first characterize the TiN thin films of different thicknesses by measuring sheet resistance $R_\square$ as a function of temperature T. $R_\square$ were measured using standard low-frequency four-terminal lock-in measurement technique, with bias current kept low enough to avoid Joule heating, and below the critical current of the superconducting state. Superconducting transitions were observed in films with thickness down to $t = 3$ nm [Supplementary Fig. S2]. From these measurements, we extract the

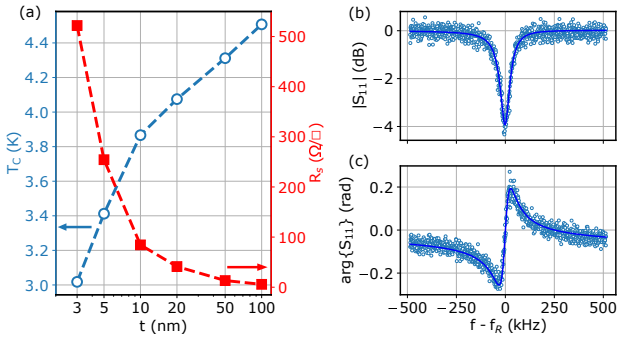

Figure 1. (a) Superconducting transition temperature T_C (blue open circles, left axis) and normal state sheet resistance R_s (red filled squares, right axis) obtained just before superconducting transitions versus TiN film thickness t. The dashed lines are guides to the eye. (b) Magnitude (top pannel) and phase (bottom pannel) of S_{11} parameter of a TiN microwave resonator with $t = 3$ nm, with resonance frequency $f_R = 5.563$ GHz measured using a 3D waveguide. We extract $Q_i = 0.9 \times 10^5$, $Q_c = 4.1 \times 10^5$ and $< n >= 1.3$ from the fit (blue thick line) to the data points [44].

normal-state sheet resistance R_s [Fig. 1(a)], which is the value of $R_\square$ obtained just before the superconducting transition. R_S increases by nearly two orders of magnitude as the film thickness reduces; from 5.7 Ω/□ observed for $t = 100$ nm film to 522.0 Ω/□ in $t = 3$ nm film. We then extract the superconducting transition temperature T_c [Fig. 1(a)], defined as T at which $R_\square$ drops below 1.0 % of R_s. The T_c decreases from 4.5 K measured for $t = 100$ nm film to 3.3 K for $t = 3$ nm film. Such decrease in T_C with decreasing t is common in disordered thin-film superconductors [45]. The residual-resistance-ratio RRR defined as $RRR = R_\square(300\ K)/R_s$ is a measure of disorder present in thin films and characterizes film quality. The largest value of RRR=1.3 observed for the $t = 100$ nm film is similar to RRR typically reported in high quality TiN thin films [46, 47]. In Tbl. I, we summarize different characteristic parameters of our TiN thin films.

Table I. Thin film characteristics

Thickness (nm)	RRR	T_C (K)	R_S (Ω/□)	L_K (pH/□)
3	1.10	3.0	522.0	239.0
5	1.17	3.4	254.4	103.0
10	1.17	3.9	93.5	33.4
20	1.23	4.1	41.2	14.0
50	1.25	4.3	13.3	4.2
100	1.33	4.5	5.7	1.7

We then designed multiple microstrip $\lambda/2$ microwave resonators of different film thicknesses and aspect ratio; a total of 4 resonators using 3 nm film, 7 resonators using 5 nm film, and 6 resonators using 10 nm films, and measured complex scattering parameters with a vector network analyzer, both in planar microstrip geometry (refered to as 2D later on) and rectangular 3D waveguide [see Supplementary section-IV for details]. All the microwave measurements described below have been performed at the base temperature of the dilution refrigerator of 25 mK, unless otherwise specified. We obtain coupling quality factor Q_C, internal quality factor Q_i and mode frequency f_R by fitting the data with standard fit procedures [44]. The average photon number n circulating in the resonator is estimated using $n = P_{in}Q_l^2/(\hbar\pi^2)f_R^2Q_C$, where P_{in} is the attenuated input power, and the loaded quality factor $Q_l^{-1} = Q_i^{-1} + Q_C^{-1}$. In Fig. 1(b-c), we show representative plots of magnitude (Fig. 1(b)) and phase of (Fig. 1(c)) reflection parameter S_{11}, for a $t = 3$ nm TiN resonator measured in a 3D waveguide. From the fit to the datapoints, we obtain $Q_i \sim 0.9 \times 10^5$, measured in the single photon limit. $Q_i \sim 10^5$ in the single photon limit for such a thin film (~ 3 nm) high kinetic inductance resonator is comparable to the best values reported thus far [27, 31, 48–50].

Sheet kinetic inductance L_K of a disordered superconductor scales inversely with superfluid density in the material. We obtain consistent L_K using both DC and microwave characterizations, as described below. We measure resonators with length 6.5 mm and width of 2 μm and different film thicknes t and thus different L_K, which exhibit multiple modes; *e.g.* 10 modes were observed with $t = 3$ nm resonator [supplementary Fig. S6]. The mode dispersion deviates progressively from expected linear behaviour at higher f_R. The experimental dispersion fits with a modified version of long-range Coulomb interaction model [20], developed taking into account the charge screening by the presence of a ground plane at the back of the device chip [51]. We extract L_K from the fit, which is the only fit parameter in the model. We also perform a finite-element electromagnetic simulation using Sonnet®, and obtain f_R for our specific device geometry, and different values of L_K, which is an input parameter in the simulations. The experimentally obtained f_R is then used to fit into this simulated f_R versus L_K relationship, and estimate the L_K for our TiN films. Finally, we also extract L_K of the films from the resistivity measurements [shown in Fig. 1] using $L_K = \hbar R_S/\pi\Delta_0$ [27, 28], where the $T = 0$ superconducting gap is obtained using the BCS relationship $\Delta_0 = 1.76 k_B T_C$. Fig. 2 plots L_K obtained from all the above mentioned measurements, for different t, showing excellent agreement between the three different methods. We emphasize here that all the DC and microwave measurements presented until now and to be discussed later for a specific t are carried out from dif-

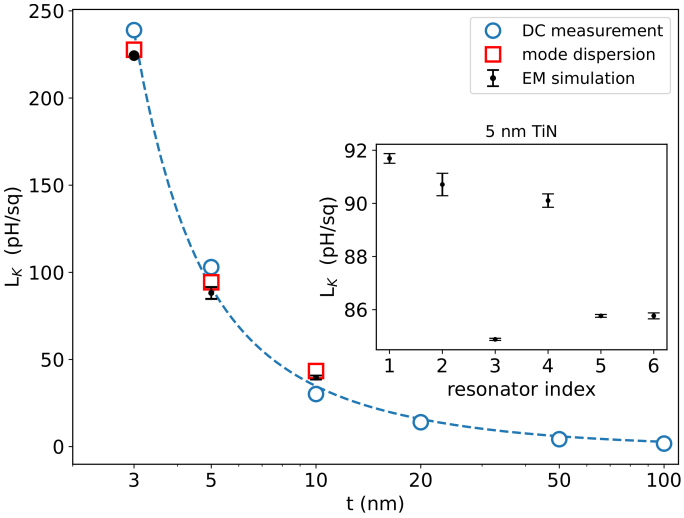

Figure 2. Sheet kinetic inductance L_K versus TiN film thickness t. The blue dashed line is a guide to the eye. L_K computed from superconducting transition temperature T_C and normal state sheet resistance R_s as $L_K = \hbar R_s/1.76\pi k_B T_C$ is plotted with blue open circles. L_K obtained from resonance frequency versus mode number dispersion relation for microstrip $\lambda/2$ resonators are shown with red open box. In black filled circles, we show plots of L_K obtained from electromagnetic simulation using Sonnet®, where L_K were tuned as a parameter of simulation to match mode frequency f_R for a resonator of a given dimensions with experimentally obtained f_R. The errorbars represent spread in absolute value of the estimation from multiple resonators of different dimensions. Inset: Plots of L_K, obtained using third method, from 6 different microwave resonators made with 5 nm TiN film, show a spread of less than 8% in L_K. The errorbars are estimated using resonance linewidth as an error estimate for f_R of the observed resonance.

ferent parts of 200 mm diameter wafers. The agreement of L_K over all such measurements indicates excellent homogeneity of the stoichiometry and thickness, which is an asset of VLSI fabrication.

For the $t = 100$ nm film, we obtain very small value of $L_K = 1.0$ pH/□, at the limit where L_K contributes negligibly to the total inductance. L_K increases with decreasing t, reaching a significant value of 239 pH/□ (Tbl. I) for $t = 3$ nm, two orders of magnitude larger than the value for $t = 100$ nm film. This increase in L_K with decrease in t is a consequence of reduction of superfluid density in the superconducting state. Our observation of such an increase in the L_K with decreasing t is in qualitative agreement with TiN films deposited using other methods [27] and other disordered thin-film superconductors.

While we obtain large value of L_K for thin TiN films, stability and low-loss at microwave frequencies are basic requirements for a scalable quantum technology platform. As a result of high film quality, as characterized above [also Supplementary section-III], we observed excellent long term stability of microwave resonators, characterized as minimal shift in resonance frequencies measured over time period of several months [Supplementary Fig. S7], contrary to what is often observed in very thin films.

A very common source of loss in superconducting quantum devices are two-level systems (TLS) [52]. A series of detailed investigations showed that impurities residing at the metal-substrate interface is the major contributor to the TLS losses. This can be attributed to the order of magnitude larger participation of stored electric field in metal-substrate interfaces, as compared to metal-air or substrate-air interfaces [52]. On the other hand, as the kinetic inductance fraction $\alpha = L_{kinetic}/L_{total}$ approaches unity, susceptibility to quasiparticles (QP), and in turn, induced microwave losses due to QP increases [31, 53]. Non-equilibrium quasiparticles in high kinetic inductance granular aluminum resonators have been found to be the dominant source of microwave losses [31, 49, 50]. We study the evolution of Q_i of multiple TiN resonators, both in planar microstrip geometry and in rectangular 3D waveguide achieving different metal-substrate participation ratio p_{ms}, with variation of microwave power and temperature to unravel the underlying loss mechanisms.

Q_i for a $t = 5$ nm resonator increases, from $Q_i \sim 2.0 \times 10^5$ measured at single photon limit, by ~ 2 times to $Q_i \sim 4.5 \times 10^5$ over four orders of magnitude increase in the photon number n, and then tends to saturate [Fig. 3(a)]. In the inset of Fig. 3(a), we show plots of Q_i versus n, measured for a resonator made with $t = 3$ nm TiN. We observe here distinct behaviours for the Q_i versus n for this two different thicknesses. For 3 nm TiN, we observe $Q_i \sim 0.9 \times 10^5$ in the single photon limit, which indicates larger loss in the $t = 3$ nm resonators as compared to $t = 5$ nm resonators. Over the three orders of magnitude increase in n, Q_i shows only a weak dependence on n for the $t = 3$ nm resonator. Such larger losses in $t = 3$ nm resonator as compared to $t = 5$ nm resonator have been consistently observed over multiple resonators with different f_R and aspect ratios, while the substrate and the entire fabrication procedure remained the same.

To gain more insight, In Fig. 3(b), we combine Q_i in the single photon limit versus p_{ms}, computed following standard methodology [54–56], for our TiN resonators [filled circles and squares] and also from literature survey of resonators [open squares and pentagons], and transmon qubits dominated by capacitive losses. The dashed lines represent an empirical relation of $Q_i = [p_{ms} \tan\delta]^{-1}$, being governed solely by dielectric loss in substrate quantified by the $\tan\delta$ parameter.

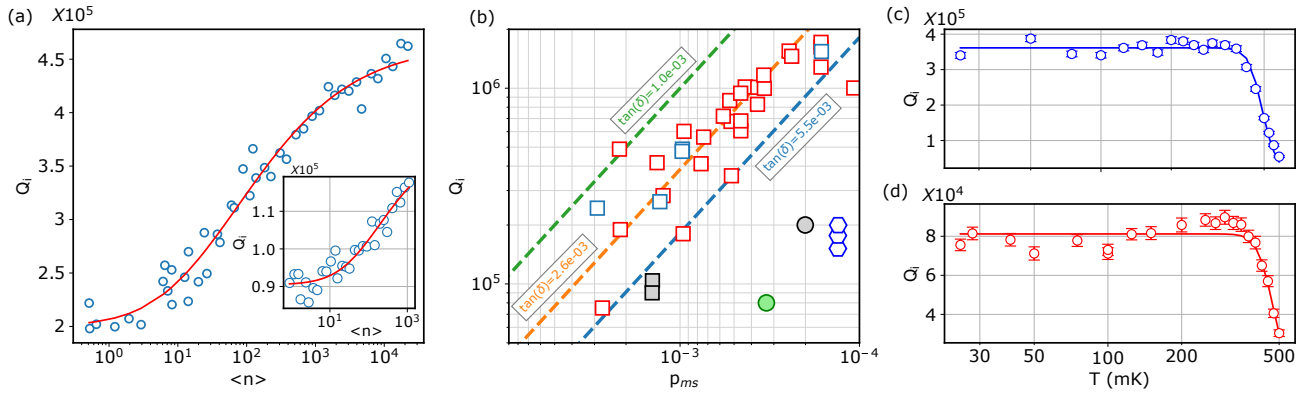

Figure 3. Microwave losses in TiN resonators. (a) Internal quality factor Q_i versus average photon number n measured for a $t = 5$ nm resonator. The blue open circles are the data points while the red lines are fit to the data points using QP (Supplementary Eqn. S1) induced loss model. Right-bottom inset: Q_i versus n measured for a $t = 3$ nm resonator (blue open circles), and fit to the data points, similar to that shown in the main panel. (b) Q_i versus metal-substrate participation ratio. The open squares represent superconducting microwave resonators and transmon qubits from literature [red squares from Ref. [54] and blue squares from Ref. [31]]. Open pentagons represent high kinetic inductance granular aluminum microwave resonators [31], in which Q_i were limited by quasiparticle loss. Our microwave resonators are represented by black (5 nm TiN) and green (3 nm TiN) filled squares and circles. The black filled squares correspond to Q_i of 2D microstrip resonators, while filled circles represent Q_i of resonators measured using rectangular 3D waveguide. The dashed lines represent $Q_i = [p_{ms} \tan\delta]^{-1}$ for three different values of dielectric loss tangent $\tan\delta$, in range with typically measured values for high quality Si or sapphire substrates [31, 54–56]. (c-d) Temperature dependence of losses in TiN microwave resonators. Plots of Q_i versus T measured for (c) $t = 5$ nm (d) and $t = 3$ nm TiN resonators. The thick lines are fit to the data using Eqn. 1, which takes into account thermally induced quasiparticles.

A cluster of data points from literature [open square], for which the dominant loss is from two-level systems at metal substrate interface, obeys this empirical relation. Q_i in our 2D (planar) microstrip TiN resonator [black filled square] match well with predicted value obtained using $\tan\delta \sim 5.5 \times 10^{-3}$, which is typical for standard high-quality Si substrates. However, a far-away ground plane provided by the metal body of a 3D rectangular waveguide significantly reduces p_{ms} by diluting the electric field in the substrate. We observe that the measured Q_i is limited to $\sim 10^5$, one order of magnitude less than that predicted by $Q_i = [p_{ms} \tan\delta]^{-1}$. Similar suppression of Q_i by orders of magnitude compared to the predicted $[p_{ms} \tan\delta]^{-1}$ were observed in high kinetic inductance granular aluminum resonators measured in similar 3D waveguides [pentagons]. The losses in this case were found to be dominated by quasiparticles [31]. For large p_{ms} ($\geq 10^{-3}$, [black filled squares]) the dominant loss is naturally from TLS at metal-surface interface, as any other loss mechanisms are masked off. On the other hand, as the p_{ms} is reduced for the resonators measured in 3D waveguide [filled circles], larger suppression of Q_i than predicted by $Q_i = [p_{ms} \tan\delta]^{-1}$ clearly suggests that other loss mechanisms become progressively dominant for high kinetic inductance TiN resonators. We obtain excellent fit to the n dependance of Q_i with the model of n-dependent loss due to localized QP [31] [see Supplementary section-VI for details], which suggests that QP induced losses are probably the dominant loss mechanism in our resonators, similar to previous observations in high kinetic inductance resonators [31, 50, 57]. QP can be generated in these devices because of photons, phonons or other high-energy particles, and often manifest as sudden frequency jumps of the resonators by 'bursts' of quasiparticles. However, identifying the exact origin of these QP is an active field of research, and beyond the scope of this work.

We then studied the temperature dependance of the losses to gain more insight into the various mechanisms possibly at stake. Q_i remains essentially T independent until about 400 mK, and then decreases monotonously, but sharply with further increasing T [Fig. 3(c-d)]. As T increases, the thermal equilibrium quasiparticle density n_{qp} increases [58, 59], as given by $n_{qp}(T) = D(E_F)\sqrt{2\pi k_B T \Delta}\exp(\Delta_0/k_B T)$, where $D(E_F)$ is the density of states at the Fermi energy, and Δ_0 is the superconducting gap at $T = 0$. The increasing n_{qp} results in additional loss in microwave resonators, governed by:

$$\frac{1}{Qi} = 2\alpha\sqrt{\frac{k_B T}{\pi h f_R}}\exp\left(-\frac{\Delta_0}{k_B T}\right) + \frac{1}{Q_a} \qquad (1)$$

with $\alpha = L_{kinetic}/L_{total}$ being the kinetic inductance fraction, and $\frac{1}{Q_a}$ is loss because of other loss mechanisms, which, in our case, is dominated by loss due to non equilibrium localized QP, as discussed previously. Δ_0 obtained from the fits to the data [thick lines in Fig. 3(c-d)]

using Eqn. 1, with $\alpha = 1$ and Δ_0 being the only free parameter, agrees well within 10% uncertainty [27, 60] with the BCS prediction of $1.76 k_B T_C$. We note here that, observed saturation in Q_i for $T \leq 400$ mK is contrasting to TLS predictions, where saturation of TLS because of provided thermal energy results in an increase in Q_i. Hence the measured T dependance of Q_i is in agreement with the previous discussion suggesting that the microwave loss in the single photon limit in TiN resonators in 3D waveguide is not predominantly TLS limited but rather due to the presence of non-equilibrium quasiparticles.

The total kinetic inductance of a superinductor of length l and width w can be estimated as $L_{kinetic} = \frac{l}{w} L_K = \frac{\hbar}{1.76\pi k_B} \frac{l}{w} \frac{R_N}{T_C}$, whereas, in the limit of $l \gg w \gg t$, t being the thickness, the geometric inductance can be approximated to $L_{geo} \approx \frac{\mu_0}{2\pi} l \ln(\frac{2l}{w})$ [57, 61]. For our $t = 3$ nm TiN resonator, we obtain $L_{kinetic} = 290$ nH, which is comparable to typical values of ~ 100 nH of high-impedance superinductors used in high-coherence fluxonium qubits [13, 21, 42, 62]. We also obtain $\alpha = 0.98$ and $\alpha = 0.99$ for $t = 5$ nm and $t = 3$ nm TiN resonators, respectively, justifying the constraints $\alpha = 1$ in the fit in Fig. 3(c-d). Such large L_K, or equivalently $\alpha \sim 1$, is key towards obtaining high characteristic impedance. We estimate impedance $Z_c = \sqrt{\mathcal{L}/c}$, where $\mathcal{L}$ and c are inductance and capacitance per unit length of the resonator, of 3.2 kΩ for our $t = 3$ nm TiN resonator, measured in the 3D waveguide. We measure Z_c as high as 4.2 kΩ for a $t = 3$ nm TiN resonator with $f_R = 8.7$ GHz in a 2D geometry [see Supplementary section-VII for details]. Z_c can be further modulated by modifying l/w of the resonator.

In summary, we studied the microwave properties of superconducting TiN thin films fabricated with a VLSI platform. We showed that the films remain superconducting down to at least 3 nm, with a critical temperature still exceeding 3 K. When reducing the film thickness, the kinetic inductance increases up to 239 pH/□ for a 3 nm thick film. In microwave resonators, we demonstrate very large total inductance of several hundreds of nH and characteristic impedance $Z_c \approx 4.2$ kΩ together with state-of-the-art losses in the single photon regime, *i.e.* internal quality factors $Q_i \approx 10^5$. We show evidence that the remaining losses can be attributed to non-equilibrium quasiparticles. Mitigation strategies, such as an improved shielding or phonon traps might help to reduce the losses even further in the future. Our TiN showed negligible degradation due to aging, contrary to what is often observed in very thin films. All these demonstrations open up the possibility to develop industrial scale fabrication of superconducting microwave circuits. The compatibility of TiN with large magnetic field will also allow to integrate it into hybrid circuits using semiconductor spins and superconducting circuits.

This work was supported by the French National Research Agency (ANR) in the framework of the Graphmon project (ANR-19-CE47-0007) and the QNEMS project from LETI Carnot Institute. JR acknowledges F. Balestro, V. Bouchiat, E. Eyraud and W. Wernsdorfer for help with the cryogenic system. KRA acknowledge help of F. Faroughi in EM simulations and with 3D waveguide. We acknowledge the help of P. Lachkar for DC resistivity measurements. We acknowledge the work of J. Jarreau and L. Del-Rey for the fabrication of the 3D waveguide. We acknowledge support from the Nanofab team of Institut Néel, and from Guillaume Rodriguez of CEA Leti.

[1] F. Arute, K. Arya, R. Babbush, D. Bacon, J. C. Bardin, R. Barends, R. Biswas, S. Boixo, F. G. S. L. Brandao, D. A. Buell, B. Burkett, Y. Chen, Z. Chen, B. Chiaro, R. Collins, W. Courtney, A. Dunsworth, E. Farhi, B. Foxen, A. Fowler, C. Gidney, M. Giustina, R. Graff, K. Guerin, S. Habegger, M. P. Harrigan, M. J. Hartmann, A. Ho, M. Hoffmann, T. Huang, T. S. Humble, S. V. Isakov, E. Jeffrey, Z. Jiang, D. Kafri, K. Kechedzhi, J. Kelly, P. V. Klimov, S. Knysh, A. Korotkov, F. Kostritsa, D. Landhuis, M. Lindmark, E. Lucero, D. Lyakh, S. Mandrà, J. R. McClean, M. McEwen, A. Megrant, X. Mi, K. Michielsen, M. Mohseni, J. Mutus, O. Naaman, M. Neeley, C. Neill, M. Y. Niu, E. Ostby, A. Petukhov, J. C. Platt, C. Quintana, E. G. Rieffel, P. Roushan, N. C. Rubin, D. Sank, K. J. Satzinger, V. Smelyanskiy, K. J. Sung, M. D. Trevithick, A. Vainsencher, B. Villalonga, T. White, Z. J. Yao, P. Yeh, A. Zalcman, H. Neven, and J. M. Martinis, Quantum supremacy using a programmable superconducting processor, Nature **574**, 505 (2019).

[2] Y. Wu, W.-S. Bao, S. Cao, F. Chen, M.-C. Chen, X. Chen, T.-H. Chung, H. Deng, Y. Du, D. Fan, M. Gong, C. Guo, C. Guo, S. Guo, L. Han, L. Hong, H.-L. Huang, Y.-H. Huo, L. Li, N. Li, S. Li, Y. Li, F. Liang, C. Lin, J. Lin, H. Qian, D. Qiao, H. Rong, H. Su, L. Sun, L. Wang, S. Wang, D. Wu, Y. Xu, K. Yan, W. Yang, Y. Yang, Y. Ye, J. Yin, C. Ying, J. Yu, C. Zha, C. Zhang, H. Zhang, K. Zhang, Y. Zhang, H. Zhao, Y. Zhao, L. Zhou, Q. Zhu, C.-Y. Lu, C.-Z. Peng, X. Zhu, and J.-W. Pan, Strong quantum computational advantage using a superconducting quantum processor (2021), arXiv:2106.14734 [quant-ph].

[3] P. Forn-Díaz, L. Lamata, E. Rico, J. Kono, and E. Solano, Ultrastrong coupling regimes of light-matter interaction, Rev. Mod. Phys. **91**, 025005 (2019).

[4] A. Frisk Kockum, A. Miranowicz, S. De Liberato, S. Savasta, and F. Nori, Ultrastrong coupling between light and matter, Nature Reviews Physics **1**, 19 (2019).

[5] S. Léger, J. Puertas-Martínez, K. Bharadwaj, R. Dassonneville, J. Delaforce, F. Foroughi, V. Milchakov, L. Planat, O. Buisson, C. Naud, W. Hasch-Guichard, S. Florens, I. Snyman, and N. Roch, Observation of quantum many-body effects due to zero point fluctuations in superconducting circuits, Nature Communications **10**, 5259 (2019).

[6] R. Kuzmin, N. Mehta, N. Grabon, R. Mencia, and V. E. Manucharyan, Superstrong coupling in circuit quantum electrodynamics, npj Quantum Information **5**, 20 (2019).

[7] P. Roushan, C. Neill, J. Tangpanitanon, V. M. Bastidas, A. Megrant, R. Barends, Y. Chen, Z. Chen, B. Chiaro, A. Dunsworth, A. Fowler, B. Foxen, M. Giustina, E. Jeffrey, J. Kelly, E. Lucero, J. Mutus, M. Neeley, C. Quintana, D. Sank, A. Vainsencher, J. Wenner, T. White, H. Neven, D. G. Angelakis, and J. Martinis, Spectroscopic signatures of localization with interacting photons in superconducting qubits, Science **358**, 1175 (2017).

[8] R. Ma, B. Saxberg, C. Owens, N. Leung, Y. Lu, J. Simon, and D. I. Schuster, A dissipatively stabilized mott insulator of photons, Nature **566**, 51 (2019).

[9] I. Carusotto, A. A. Houck, A. J. Kollár, P. Roushan, D. I. Schuster, and J. Simon, Photonic materials in circuit quantum electrodynamics, Nature Physics **16**, 268 (2020).

[10] A. Gyenis, P. S. Mundada, A. Di Paolo, T. M. Hazard, X. You, D. I. Schuster, J. Koch, A. Blais, and A. A. Houck, Experimental realization of a protected superconducting circuit derived from the 0–π qubit, PRX Quantum **2**, 010339 (2021).

[11] A. Gyenis, A. D. Paolo, J. Koch, A. Blais, A. A. Houck, and D. I. Schuster, Moving beyond the transmon: Noise-protected superconducting quantum circuits (2021), arXiv:2106.10296 [quant-ph].

[12] V. E. Manucharyan, *Superinductance*, Ph.D. thesis, Yale University (2012).

[13] I. M. Pop, K. Geerlings, G. Catelani, R. J. Schoelkopf, L. I. Glazman, and M. H. Devoret, Coherent suppression of electromagnetic dissipation due to superconducting quasiparticles, Nature **508**, 369 (2014).

[14] V. E. Manucharyan, J. Koch, L. I. Glazman, and M. H. Devoret, Fluxonium: Single cooper-pair circuit free of charge offsets, Science **326**, 113 (2009).

[15] P. Brooks, A. Kitaev, and J. Preskill, Protected gates for superconducting qubits, Phys. Rev. A **87**, 052306 (2013).

[16] A. Stockklauser, P. Scarlino, J. V. Koski, S. Gasparinetti, C. K. Andersen, C. Reichl, W. Wegscheider, T. Ihn, K. Ensslin, and A. Wallraff, Strong coupling cavity qed with gate-defined double quantum dots enabled by a high impedance resonator, Phys. Rev. X **7**, 011030 (2017).

[17] J. Puertas Martínez, S. Léger, N. Gheeraert, R. Dassonneville, L. Planat, F. Foroughi, Y. Krupko, O. Buisson, C. Naud, W. Hasch-Guichard, S. Florens, I. Snyman, and N. Roch, A tunable josephson platform to explore many-body quantum optics in circuit-qed, npj Quantum Information **5**, 19 (2019).

[18] M. T. Bell, I. A. Sadovskyy, L. B. Ioffe, A. Y. Kitaev, and M. E. Gershenson, Quantum superinductor with tunable nonlinearity, Phys. Rev. Lett. **109**, 137003 (2012).

[19] N. A. Masluk, I. M. Pop, A. Kamal, Z. K. Minev, and M. H. Devoret, Microwave characterization of josephson junction arrays: Implementing a low loss superinductance, Phys. Rev. Lett. **109**, 137002 (2012).

[20] Y. Krupko, V. D. Nguyen, T. Weißl, E. Dumur, J. Puertas, R. Dassonneville, C. Naud, F. W. J. Hekking, D. M. Basko, O. Buisson, N. Roch, and W. Hasch-Guichard, Kerr nonlinearity in a superconducting josephson metamaterial, Phys. Rev. B **98**, 094516 (2018).

[21] L. Grünhaupt, M. Spiecker, D. Gusenkova, N. Maleeva, S. T. Skacel, I. Takmakov, F. Valenti, P. Winkel, H. Rotzinger, W. Wernsdorfer, A. V. Ustinov, and I. M. Pop, Granular aluminium as a superconducting material for high-impedance quantum circuits, Nature Materials **18**, 816 (2019).

[22] A. P. M. Place, L. V. H. Rodgers, P. Mundada, B. M. Smitham, M. Fitzpatrick, Z. Leng, A. Premkumar, J. Bryon, A. Vrajitoarea, S. Sussman, G. Cheng, T. Madhavan, H. K. Babla, X. H. Le, Y. Gang, B. JÃ€ck, A. Gyenis, N. Yao, R. J. Cava, N. P. de Leon, and A. A. Houck, New material platform for superconducting transmon qubits with coherence times exceeding 0.3 milliseconds, Nature Communications **12**, 1779 (2021).

[23] C. Wang, X. Li, H. Xu, Z. Li, J. Wang, Z. Yang, Z. Mi, X. Liang, T. Su, C. Yang, G. Wang, W. Wang, Y. Li, M. Chen, C. Li, K. Linghu, J. Han, Y. Zhang, Y. Feng, Y. Song, T. Ma, J. Zhang, R. Wang, P. Zhao, W. Liu, G. Xue, Y. Jin, and H. Yu, Transmon qubit

with relaxation time exceeding 0.5 milliseconds (2021), arXiv:2105.09890 [quant-ph].

[24] K. Makise, R. Sun, H. Terai, and Z. Wang, Fabrication and characterization of epitaxial tin-based josephson junctions for superconducting circuit applications, IEEE Transactions on Applied Superconductivity **25**, 1 (2015).

[25] M. R. Vissers, J. Gao, D. S. Wisbey, D. A. Hite, C. C. Tsuei, A. D. Corcoles, M. Steffen, and D. P. Pappas, Low loss superconducting titanium nitride coplanar waveguide resonators, Applied Physics Letters **97**, 232509 (2010), https://doi.org/10.1063/1.3517252.

[26] H. G. Leduc, B. Bumble, P. K. Day, B. H. Eom, J. Gao, S. Golwala, B. A. Mazin, S. McHugh, A. Merrill, D. C. Moore, O. Noroozian, A. D. Turner, and J. Zmuidzinas, Titanium nitride films for ultrasensitive microresonator detectors, Applied Physics Letters **97**, 102509 (2010), https://doi.org/10.1063/1.3480420.

[27] A. Shearrow, G. Koolstra, S. J. Whiteley, N. Earnest, P. S. Barry, F. J. Heremans, D. D. Awschalom, E. Shirokoff, and D. I. Schuster, Atomic layer deposition of titanium nitride for quantum circuits, Applied Physics Letters **113**, 212601 (2018), https://doi.org/10.1063/1.5053461.

[28] N. Samkharadze, A. Bruno, P. Scarlino, G. Zheng, D. P. DiVincenzo, L. DiCarlo, and L. M. K. Vandersypen, High-kinetic-inductance superconducting nanowire resonators for circuit qed in a magnetic field, Phys. Rev. Applied **5**, 044004 (2016).

[29] D. Niepce, J. Burnett, and J. Bylander, High kinetic inductance NbN nanowire superinductors, Phys. Rev. Applied **11**, 044014 (2019).

[30] C. X. Yu, S. Zihlmann, G. Troncoso Fernández-Bada, J.-L. Thomassin, F. Gustavo, E. Dumur, and R. Maurand, Magnetic field resilient high kinetic inductance superconducting niobium nitride coplanar waveguide resonators, Applied Physics Letters **118**, 054001 (2021), https://doi.org/10.1063/5.0039945.

[31] L. Grünhaupt, N. Maleeva, S. T. Skacel, M. Calvo, F. Levy-Bertrand, A. V. Ustinov, H. Rotzinger, A. Monfardini, G. Catelani, and I. M. Pop, Loss mechanisms and quasiparticle dynamics in superconducting microwave resonators made of thin-film granular aluminum, Phys. Rev. Lett. **121**, 117001 (2018).

[32] W. Zhang, K. Kalashnikov, W.-S. Lu, P. Kamenov, T. DiNapoli, and M. Gershenson, Microresonators fabricated from high-kinetic-inductance aluminum films, Phys. Rev. Applied **11**, 011003 (2019).

[33] O. V. Astafiev, L. B. Ioffe, S. Kafanov, Y. A. Pashkin, K. Y. Arutyunov, D. Shahar, O. Cohen, and J. S. Tsai, Coherent quantum phase slip, Nature **484**, 355 (2012).

[34] O. Dupré, A. Benoît, M. Calvo, A. Catalano, J. Goupy, C. Hoarau, T. Klein, K. L. Calvez, B. Sacépé, A. Monfardini, and F. Levy-Bertrand, Tunable sub-gap radiation detection with superconducting resonators, Superconductor Science and Technology **30**, 045007 (2017).

[35] P. Bonnet, F. Chiodi, D. Flanigan, R. Delagrange, N. Brochu, D. Débarre, and H. le Sueur, Strongly non-linear superconducting silicon resonators (2021), arXiv:2101.11125 [cond-mat.supr-con].

[36] J. Basset, D. Watfa, G. Aiello, M. Féchant, A. Morvan, J. Estéve, J. Gabelli, M. Aprili, R. Weil, A. Kasumov, H. Bouchiat, and R. Deblock, High kinetic inductance microwave resonators made by he-beam assisted deposition of tungsten nanowires, Applied Physics Letters **114**, 102601 (2019), https://doi.org/10.1063/1.5080925.

[37] E. F. C. Driessen, P. C. J. J. Coumou, R. R. Tromp, P. J. de Visser, and T. M. Klapwijk, Strongly disordered tin and nbtin *s*-wave superconductors probed by microwave electrodynamics, Phys. Rev. Lett. **109**, 107003 (2012).

[38] P. C. J. J. Coumou, E. F. C. Driessen, J. Bueno, C. Chapelier, and T. M. Klapwijk, Electrodynamic response and local tunneling spectroscopy of strongly disordered superconducting tin films, Phys. Rev. B **88**, 180505 (2013).

[39] M. Sandberg, M. R. Vissers, J. S. Kline, M. Weides, J. Gao, D. S. Wisbey, and D. P. Pappas, Etch induced microwave losses in titanium nitride superconducting resonators, Applied Physics Letters **100**, 262605 (2012), https://doi.org/10.1063/1.4729623.

[40] S. Ohya, B. Chiaro, A. Megrant, C. Neill, R. Barends, Y. Chen, J. Kelly, D. Low, J. Mutus, P. J. J. O'Malley, P. Roushan, D. Sank, A. Vainsencher, J. Wenner, T. C. White, Y. Yin, B. D. Schultz, C. J. Palmstrøm, B. A. Mazin, A. N. Cleland, and J. M. Martinis, Room temperature deposition of sputtered TiN films for superconducting coplanar waveguide resonators, Superconductor Science and Technology **27**, 015009 (2013).

[41] S. Verhaverbeke and J. W. Parker, A model for the etching of ti and tin in sc-1 solutions, MRS Proceedings **477**, 447 (1997).

[42] T. M. Hazard, A. Gyenis, A. Di Paolo, A. T. Asfaw, S. A. Lyon, A. Blais, and A. A. Houck, Nanowire superinductance fluxonium qubit, Phys. Rev. Lett. **122**, 010504 (2019).

[43] C. E. Murray, Material matters in superconducting qubits (2021), arXiv:2106.05919 [quant-ph].

[44] S. Probst, F. B. Song, P. A. Bushev, A. V. Ustinov, and M. Weides, Efficient and robust analysis of complex scattering data under noise in microwave resonators, Review of Scientific Instruments **86**, 024706 (2015), https://doi.org/10.1063/1.4907935.

[45] B. Sacépé, C. Chapelier, T. I. Baturina, V. M. Vinokur, M. R. Baklanov, and M. Sanquer, Disorder-Induced Inhomogeneities of the Superconducting State Close to the Superconductor-Insulator Transition, Physical Review Letters **101**, 1765 (2008).

[46] A. Torgovkin, S. Chaudhuri, A. Ruhtinas, M. Lahtinen, T. Sajavaara, and I. J. Maasilta, High quality superconducting titanium nitride thin film growth using infrared pulsed laser deposition, Superconductor Science and Technology **31**, 055017 (2018).

[47] N. Saveskul, N. Titova, E. Baeva, A. Semenov, A. Lubenchenko, S. Saha, H. Reddy, S. Bogdanov, E. Marinero, V. Shalaev, A. Boltasseva, V. Khrapai, A. Kardakova, and G. Goltsman, Superconductivity behavior in epitaxial tin films points to surface magnetic disorder, Phys. Rev. Applied **12**, 054001 (2019).

[48] P. Winkel, K. Borisov, L. Grünhaupt, D. Rieger, M. Spiecker, F. Valenti, A. V. Ustinov, W. Wernsdorfer, and I. M. Pop, Implementation of a transmon qubit using superconducting granular aluminum, Phys. Rev. X **10**, 031032 (2020).

[49] F. Henriques, F. Valenti, T. Charpentier, M. Lagoin, C. Gouriou, M. Martínez, L. Cardani, M. Vignati, L. Grünhaupt, D. Gusenkova, J. Ferrero, S. T. Skacel, W. Wernsdorfer, A. V. Ustinov, G. Catelani, O. Sander, and I. M. Pop, Phonon traps reduce the quasiparticle density in superconducting cir-

cuits, Applied Physics Letters **115**, 212601 (2019), https://doi.org/10.1063/1.5124967.

[50] L. Cardani, F. Valenti, N. Casali, G. Catelani, T. Charpentier, M. Clemenza, I. Colantoni, A. Cruciani, G. D'Imperio, L. Gironi, L. Grünhaupt, D. Gusenkova, F. Henriques, M. Lagoin, M. Martinez, G. Pettinari, C. Rusconi, O. Sander, C. Tomei, A. V. Ustinov, M. Weber, W. Wernsdorfer, M. Vignati, S. Pirro, and I. M. Pop, Reducing the impact of radioactivity on quantum circuits in a deep-underground facility, Nature Communications **12**, 2733 (2021).

[51] T. Charpentier and et. al., Manuscript under preparation.

[52] C. Müller, J. H. Cole, and J. Lisenfeld, Towards understanding two-level-systems in amorphous solids: insights from quantum circuits, Reports on Progress in Physics **82**, 124501 (2019).

[53] P. K. Day, H. G. LeDuc, B. A. Mazin, A. Vayonakis, and J. Zmuidzinas, A broadband superconducting detector suitable for use in large arrays, Nature **425**, 817 (2003).

[54] C. Wang, C. Axline, Y. Y. Gao, T. Brecht, Y. Chu, L. Frunzio, M. H. Devoret, and R. J. Schoelkopf, Surface participation and dielectric loss in superconducting qubits, Applied Physics Letters **107**, 162601 (2015), https://doi.org/10.1063/1.4934486.

[55] J. Wenner, R. Barends, R. C. Bialczak, Y. Chen, J. Kelly, E. Lucero, M. Mariantoni, A. Megrant, P. J. J. O'Malley, D. Sank, A. Vainsencher, H. Wang, T. C. White, Y. Yin, J. Zhao, A. N. Cleland, and J. M. Martinis, Surface loss simulations of superconducting coplanar waveguide resonators, Applied Physics Letters **99**, 113513 (2011), https://doi.org/10.1063/1.3637047.

[56] G. Calusine, A. Melville, W. Woods, R. Das, C. Stull, V. Bolkhovsky, D. Braje, D. Hover, D. K. Kim, X. Miloshi, D. Rosenberg, A. Sevi, J. L. Yoder, E. Dauler, and W. D. Oliver, Analysis and mitigation of interface losses in trenched superconducting coplanar waveguide resonators, Applied Physics Letters **112**, 062601 (2018), https://doi.org/10.1063/1.5006888.

[57] F. Valenti, F. Henriques, G. Catelani, N. Maleeva, L. Grünhaupt, U. von Lüpke, S. T. Skacel, P. Winkel, A. Bilmes, A. V. Ustinov, J. Goupy, M. Calvo, A. Benoît, F. Levy-Bertrand, A. Monfardini, and I. M. Pop, Interplay between kinetic inductance, nonlinearity, and quasiparticle dynamics in granular aluminum microwave kinetic inductance detectors, Phys. Rev. Applied **11**, 054087 (2019).

[58] R. Barends, J. Wenner, M. Lenander, Y. Chen, R. C. Bialczak, J. Kelly, E. Lucero, P. O'Malley, M. Mariantoni, D. Sank, H. Wang, T. C. White, Y. Yin, J. Zhao, A. N. Cleland, J. M. Martinis, and J. J. A. Baselmans, Minimizing quasiparticle generation from stray infrared light in superconducting quantum circuits, Applied Physics Letters **99**, 113507 (2011), https://doi.org/10.1063/1.3638063.

[59] J. Gao, J. Zmuidzinas, A. Vayonakis, P. Day, B. Mazin, and H. Leduc, Equivalence of the effects on the complex conductivity of superconductor due to temperature change and external pair breaking, Journal of Low Temperature Physics **151**, 557 (2008).

[60] U. S. Pracht, N. Bachar, L. Benfatto, G. Deutscher, E. Farber, M. Dressel, and M. Scheffler, Enhanced cooper pairing versus suppressed phase coherence shaping the superconducting dome in coupled aluminum nanograins, Phys. Rev. B **93**, 100503 (2016).

[61] M. Tinkham, *Introduction to Superconductivity*, 2nd ed. (Courier Corporation, 2004).

[62] M. Pita-Vidal, A. Bargerbos, C.-K. Yang, D. J. van Woerkom, W. Pfaff, N. Haider, P. Krogstrup, L. P. Kouwenhoven, G. de Lange, and A. Kou, Gate-tunable field-compatible fluxonium, Phys. Rev. Applied **14**, 064038 (2020).